# Magnetic core effects on the high-frequency behavior of transformers

Nasirpour, Farzad; Ghaffarian Niasar, Mohamad; Popov, Marjan

**DOI**
10.1016/j.ijepes.2024.110035

**Publication date**
2024

**Document Version**
Final published version

**Published in**
International Journal of Electrical Power & Energy Systems

Electrical Power and Energy Systems 159 (2024) 110035

Contents lists available at ScienceDirect

International Journal of Electrical Power and Energy Systems

journal homepage: www.elsevier.com/locate/ijepes

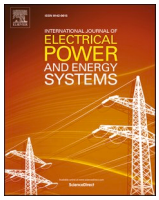

# Magnetic core effects on the high-frequency behavior of transformers

Farzad Nasirpour *, Mohamad Ghaffarian Niasar, Marjan Popov

*Delft University of Technology, Faculty of EEMCS, Delft 2628CD, the Netherlands*

ARTICLE INFO

*Keywords:*
Overvoltages
Power system transients
Power transformers
Resonances

ABSTRACT

This paper investigates the high-frequency transformer losses attributed to eddy currents in both conductors and the core. A comprehensive model of a transformer winding is presented, meticulously incorporating skin and proximity effects. The winding resistance increase due to these effects is determined by applying analytical and finite element methods. The investigation highlights that eddy current losses in the magnetic core notably increase the resistance of each winding section in low frequencies. However, the impact of these losses diminishes as the winding length approaches the voltage wavelength at high frequencies. Consequently, the net magnetomotive force and flux in the core become negligible. As a result, the high-frequency impedance characteristics are remarkably similar for windings with and without a magnetic core. These findings are substantiated through rigorous simulations and empirical measurements.

## 1. Introduction

One of the primary causes for transformer failures results from fast transient oscillations within the system [1]. When transformers are exposed to transients, the voltage distribution in their windings may become nonlinear. Additionally, these signals have the potential to trigger resonance conditions within the transformer windings, leading to a high local electric field and thus increasing the risk of failures [2]. While losses in the windings and core are undesired during normal operation, they serve to dampen and effectively limit the amplitude of the overvoltages within the transformer windings. Identifying the damping mechanisms for transient studies is crucial for transformer designers and system operators.

There are different opinions on whether conductors or magnetic core losses dominate in the high-frequency region. In [3], it is claimed that the transformer core significantly impacts the damping during transient overvoltages in transformers. Moreover, it is concluded that inductance values remain influential even for frequencies exceeding 1 MHz, contradicting the belief that flux does not penetrate the core for very high frequencies. Another research study [4] concludes that when the LV winding is open, the laminated core constitutes the primary source of loss in transformers. Authors in [5] showed that the effective complex permeability of the power transformer core is significant even at 1 MHz. By comparing the skin, proximity, and core losses, they asserted that eddy current losses in conductors are negligible. Furthermore, in [6], it is discussed that the magnetic core must be considered for frequencies above 10 kHz. All these findings show that magnetic flux exists in the core at high frequencies. In contrast, in [7], it is proposed that core losses can be disregarded due to the minimum penetration depth in transformer cores at high frequencies. Additionally, [8] suggests that the core acts as a magnetic shield at high frequencies, implying minimal losses within it.

Despite extensive research on high-frequency transformer modeling and behavior, as noted in the CIGRE workgroup A2/C4.52 [1], there is no straightforward agreement about the core effects. Therefore, through modeling, simulation, and measurement, this paper investigates the importance of conductor and core losses on the transformer's high-frequency behavior. A high-frequency model of a transformer winding is developed by considering skin, proximity, and core losses. Finite element simulations are employed to quantify the resistance increase attributable to each effect. In addition, this study investigates how high-frequency voltage wavelength minimizes core losses. These concepts are substantiated through finite element method (FEM) simulations and experimental measurements.

The rest of this paper is organized as follows: Section II provides an overview of the existing analytical method on the effects of magnetic core on conductors' resistance and inductance. Section III describes the methodology used in this study and the development of a high-frequency model that considers skin, proximity, and core losses alongside finite element simulations. Furthermore, this section elaborates on resistance increase and voltage wavelength effects at high frequencies. Section IV discusses the measurement results, and the paper ends with

* Corresponding author.
*E-mail address:* f.nasirpour@tudelft.nl (F. Nasirpour).

https://doi.org/10.1016/j.ijepes.2024.110035
Received 20 December 2023; Received in revised form 12 April 2024; Accepted 7 May 2024
Available online 15 May 2024

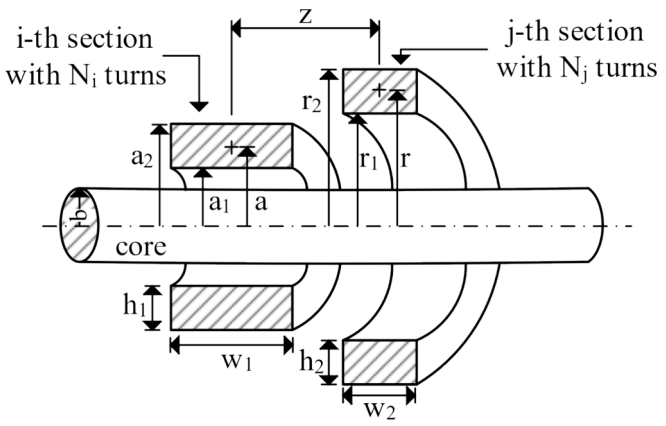


**Fig. 1.** Definition of parameters of two coils on a ferromagnetic solid core.

Section V, which summarizes the main contributions.

## 2. Core's influence on conductor resistance

When investigating transformer behavior, especially the impact of the core on winding's resistance and inductance, equations formulated by Wilcox et al. [9] play a pivotal role. These equations provide a theoretical framework for understanding the self and mutual inductances and resistances of coils wound on a solid ferromagnetic core. By solving Maxwell's equations and defining suitable boundary conditions, [9] derived equations describing the behavior of coils wound on a solid ferromagnetic core. These equations, represented by (1) through (7) for the coils wound on the same limb as shown in Fig. 1, provide insight into the relationship between the core's magnetic properties and the resulting inductances and resistances of the coils. In (1), $Z_{1(ij)}$ accounts for the effects of the common flux in the core, and it affects the sections on the same core limb equally. On the other hand, terms $Z_{2(ij)}$ and $L_{ij}$ are related to the leakage flux and influence the sections differently depending on the geometry of the transformer.

$$\mathrm{Z_{ij}} = s L_{ij} + \mathrm{Z_{1(ij)}} + \mathrm{Z_{2(ij)}} \tag{1}$$

where

$$\mathrm{Z_{1(ij)}} = s\mathrm{N_i N_j}\frac{\pi \mathrm{b}^2}{\lambda}\left\{\frac{2\mu_z \mathrm{I_1(mb)}}{\mathrm{mbI_0(mb)}} - \mu_1\right\} \tag{2}$$

$$\mathrm{Z_{2(ij)}} = s\mathrm{N_i N_j}\frac{\pi}{\lambda}\frac{4}{\mathrm{h_1 h_2 w_1 w_2}}\sum_{n=1}^{N}\left\{\begin{array}{c}\mathrm{P_1}(\beta_n \mathrm{a_1}, \beta_n \mathrm{a_2}) \times \mathrm{P_1}(\beta_n \mathrm{r_1}, \beta_n \mathrm{r_2}) \times \ \mathrm{Q_1}(\beta_n \mathrm{w_1}, \beta_n \mathrm{w_2}) \\ \times \frac{\mathrm{I_1}(\beta_n \mathrm{b})\mathrm{F_1}(\beta_n \mathrm{b})}{\mathrm{K_1}(\beta_n \mathrm{b})} \times \cos(\beta_n \mathrm{z})\end{array}\right\} \tag{3}$$

$$\mathrm{m} = \sqrt{\frac{s\mu_z}{\rho}} \tag{4}$$

$$\beta_n = \frac{2\pi \mathrm{n}}{\lambda} \tag{5}$$

In the equations above, $s$ is the Laplace variable, $\lambda$ is the apparent magnetic circuit length seen by section $i$, $\mu_z$ and $\mu_1 (\cong \mu_0)$ are the magnetic permeability of the core in the axial direction and magnetic permeability of the medium outside of it, and $\rho$ is the resistivity of the core. $I_0$, $K_0$, and $K_1$ as well as $K_1$ represent modified Bessel functions. The ancillary functions $P_1$, $Q_1$ and $F_1$ are defined in Appendix A. The choice of $N$ depends on the required level of accuracy. $L_{ij}$ can be estimated using (6):

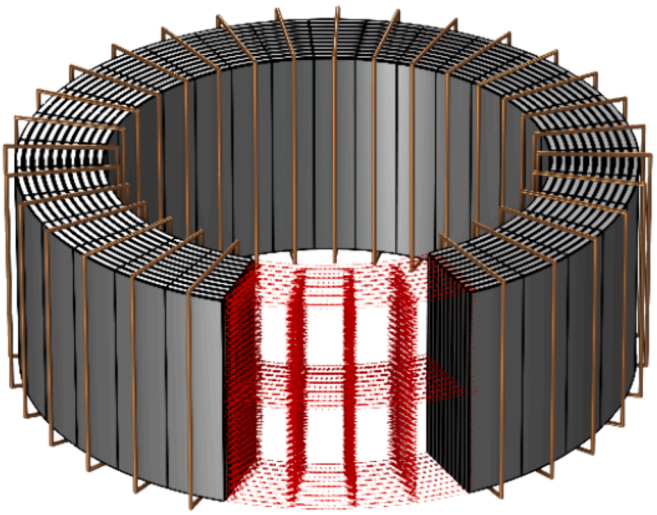

**Fig. 2.** The geometry of the laminated core.

**Table 1**
Geometry of the laminated core shown in Fig. 2.

| | |
|---|---|
| Number of turns | 32 |
| Laminated sheet width (mm) | 0.3 |
| Insulation width between sheets (mm) | 0.1 |
| Core Conductivity (S/m) | 1.12e7 |
| Inner/ outer diameter (mm) | 20/27.8 |
| Core height (mm) | 1 |
| Core relative permeability | 4000 |
| Current source (A) | 1 |

$$L_{ij} \cong \mu_0 N_i N_j \sqrt{ra}\,\frac{2}{k}\left[\left(1 - \frac{k^2}{2}\right)K(k) - E(k)\right] \tag{6}$$

where

$$k = \sqrt{\frac{4ar}{z^2 + (a+r)^2}} \tag{7}$$

Other parameters are defined in Fig. 1.

The transition from a solid core to a laminated core design necessitates deriving an equivalent solid core model. The equation proposed in [10] introduces the concept of effective conductivity ($\sigma^*$) for the solid core, providing a bridge between the laminated sheet configuration and an equivalent solid core. This concept involves replacing the laminated core with a solid equivalent exhibiting the same behavior and losses.

$$\sigma^* = \frac{\sigma k}{n^2} \tag{8}$$

In (8), $\sigma$ is the conductivity of the material the sheets are made of, $k$ is the stacking factor to account for the gaps between laminated sheets,

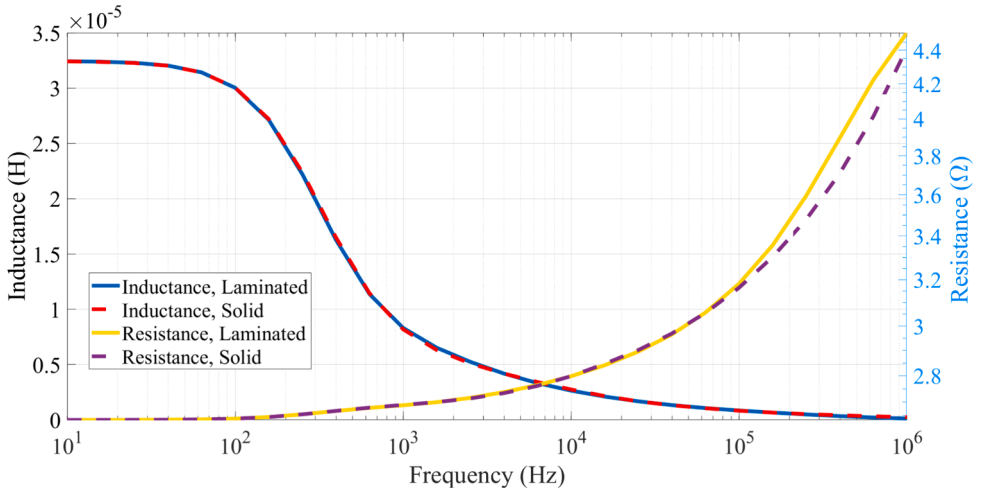


**Fig. 3.** Self-inductance and resistance of winding considering solid and laminated cores.

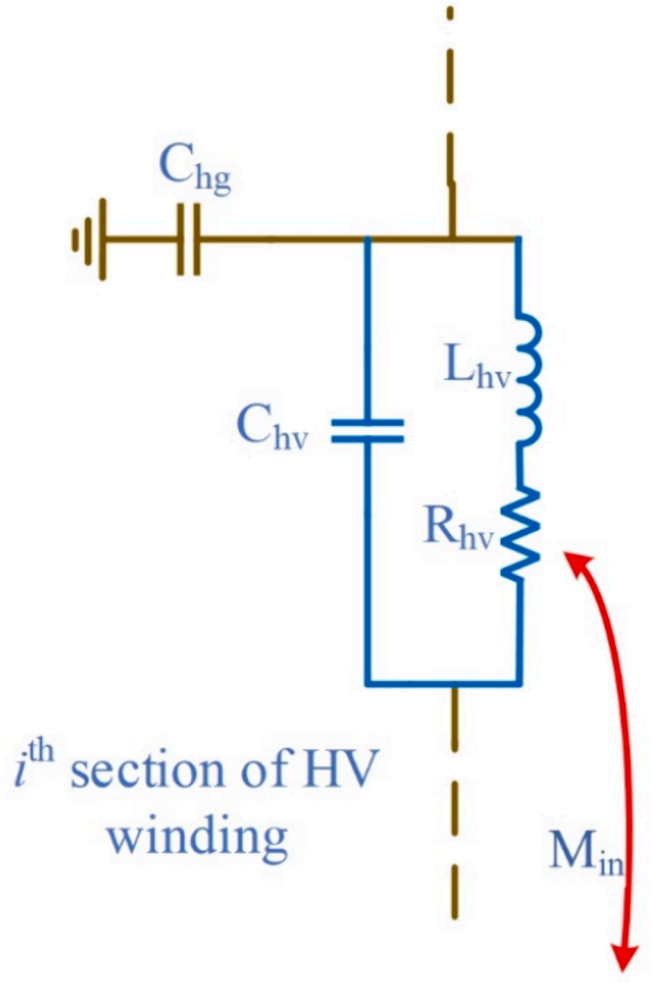


**Fig. 4.** An illustration of a section model.

and $n$ is the number of sheets.

To assess the precision of this method, FEM simulations are conducted in COMSOL Multiphysics using the magnetic field module. To manage computational resources efficiently, a small, laminated core composed of 10 sheets, each with a width of 0.3 mm made of iron, is modeled alongside its equivalent solid core (Fig. 2). Table 1 outlines the

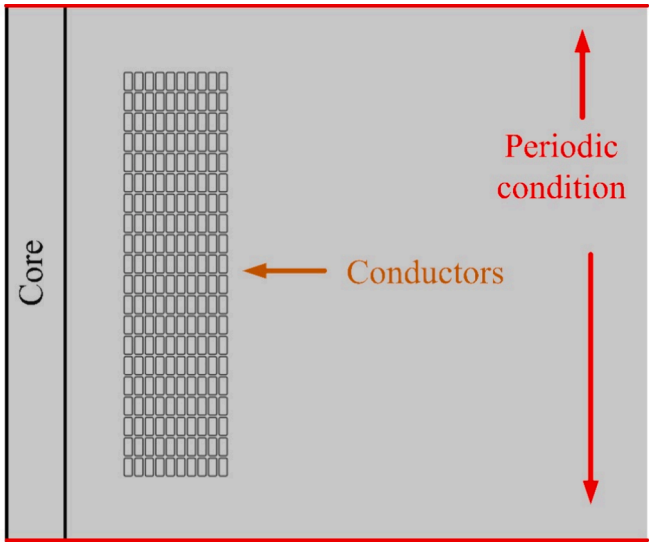


**Fig. 5.** The geometry of the winding used for the simulations.

geometric details and simulation configurations for this specific case. A copper conductor is wound around these cores. The conductor is excited with a current source, enabling the extraction of the model's inductance and resistance at various frequencies using Eqs. (9) and (10):

$$L_i = im\left(\frac{V}{\omega I}\right) \tag{9}$$

$$R_i = re\left(\frac{V}{I}\right) \tag{10}$$

Fig. 3 depicts the resulting comparisons of self-inductance and resistance of the winding, illustrating an excellent agreement between the results obtained for the laminated core and its equivalent solid core representation calculated using (8). Replacing the laminated core with an equivalent solid core model offers several advantages. Not only does it facilitate the application of analytical formulas, but also it improves significantly the mesh structure in FEM simulations, as it eliminates the need to explicitly consider the laminated structure, thereby enhancing computational efficiency and accuracy. Using this approach, the inductance and resistance of windings considering the effects of the core can be obtained.

**Table 2**
The details of disk-type winding.

| | | |
|---|---|---|
| HV winding | Winding type | Disk |
| | Number of Disks | 20 |
| | Number of turns per disk | 10 |
| | Conductor size (radial x axial) (mm) | 6.99 × 15.35 |
| | Inner/ outer diameter (mm) | 200/376 |
| Core | Leg diameter (mm) | 100 |
| | Leg height (m) | 1.2 |

## 3. Winding model

Transformer models can be broadly categorized into three main types based on the level of information required about the transformer's internal design and construction [11]: white-box models that require detailed knowledge of the transformer's geometry and construction, black-box models that rely solely on terminal measurements or frequency response data, and gray-box models that aim to derive physical models from limited geometric information typically provided by manufacturers [12]. To explore the impact of losses in both the core and conductors, a detailed high-frequency model of the transformer winding is developed, as depicted in Fig. 4. In this model, L, M, C, and R, are the self and mutual inductances, capacitances, and resistances of each section of the transformer windings. Given the focus on eddy current losses, this study excludes losses in dielectrics. The resistance R encompasses the skin and proximity effects of the conductors, along with eddy current losses in the core. These effects are outlined as follows:

- Skin effect: Eddy currents induced in the conductors, driven by the same current flow, concentrate current at the edges, leading to AC resistance increase.
- Proximity effect: Currents within one conductor induce eddy currents in nearby conductors and further increase the AC resistance.
- Eddy current in the core: Eddy currents circulating within the magnetic core contribute to increased winding resistance.

Apart from the methodology described in the previous section, FEM is used to accurately capture the combined effects of skin and proximity effects on the high-frequency winding resistance across all conductors in the winding sections. It should be noted that *the eddy currents in the conductors are not considered* in the Wilcox method.

The modeling is performed by considering a disk-type winding comprising twenty disks with ten turns each. The model is represented in a 2D domain within the FEM environment, as shown in Fig. 5, considering each disk as an individual section. Table 2 outlines the parameters required to model the winding and core. Periodic boundary conditions are applied to the upper and lower boundaries, effectively closing the core and ensuring continuity of the magnetic potential between these boundaries. By individually exciting each winding section, the self and

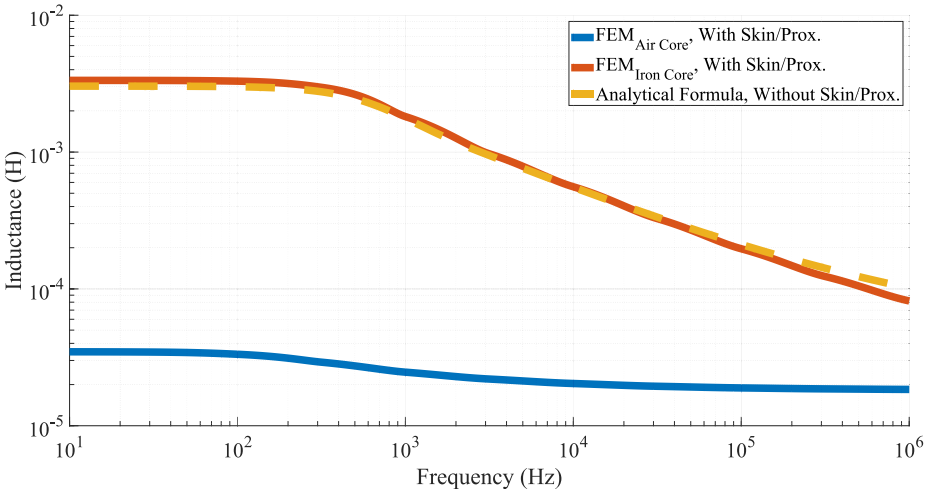


**Fig. 6.** The Self-inductance of section 1 of the winding considering air and iron cores.

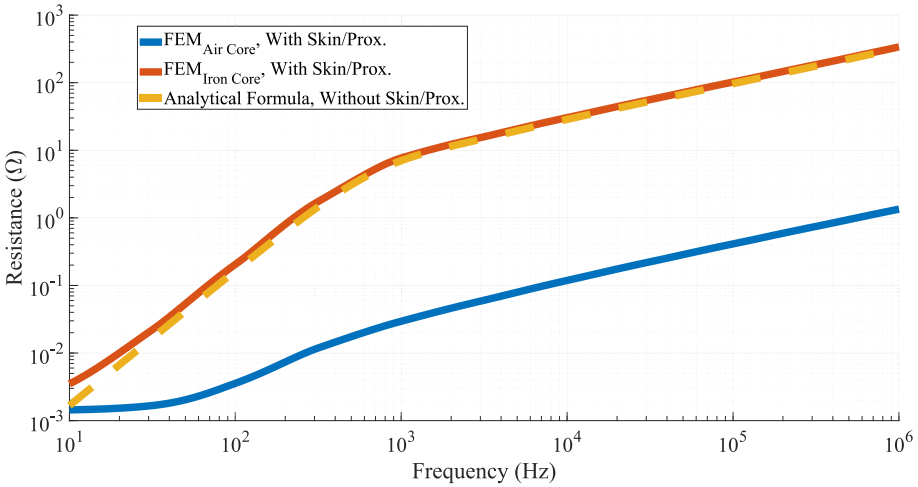


**Fig. 7.** The resistance of section 1 of the winding considering air and iron cores.

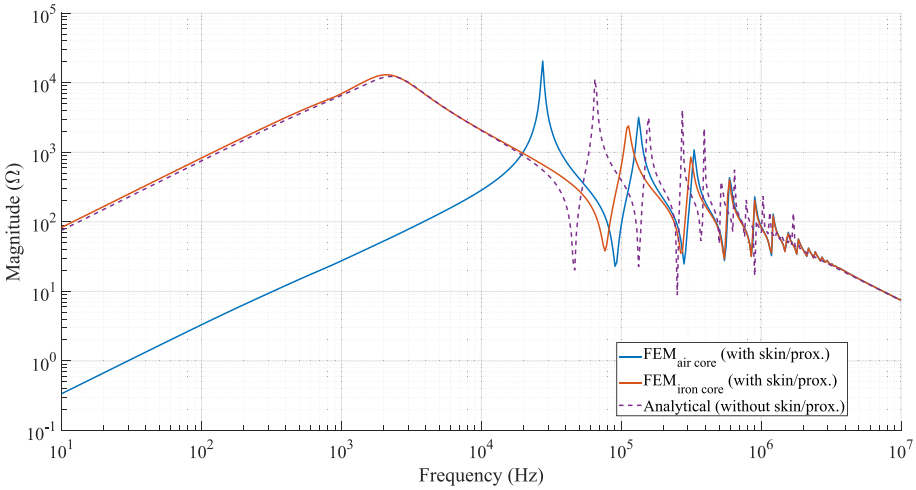


**Fig. 8.** Impedance characteristics of the winding.

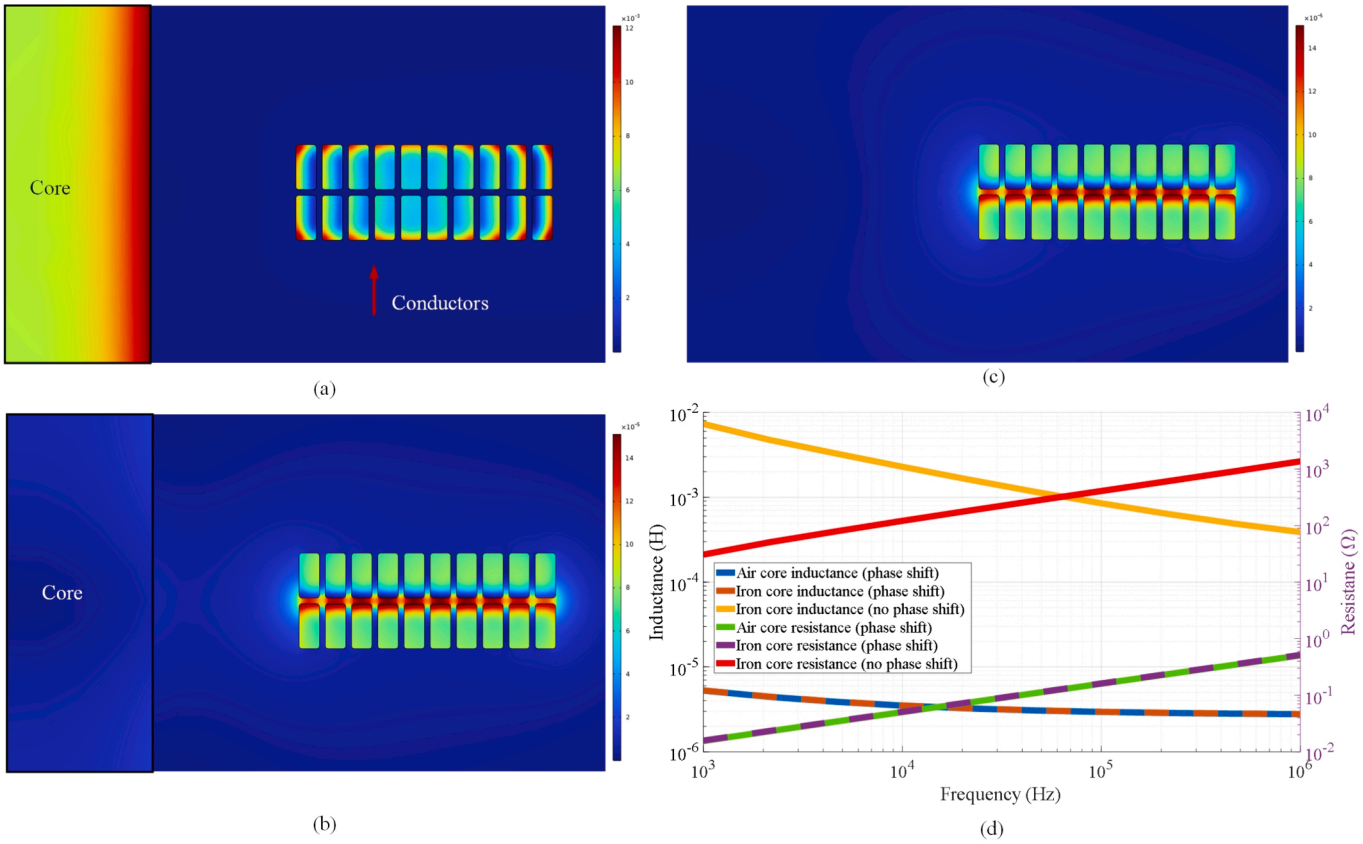


**Fig. 9.** (a) Disk carrying the same current in the presence of the magnetic core, (b) Disk carrying an opposite current in the presence of the magnetic core, (c) Disk carrying an opposite current in the air, (d) The inductance and resistance of the winding in different cases.

mutual inductances and resistances of each section are derived. These values are calculated for both ferromagnetic and air core scenarios, with and without accounting for skin and proximity effects in the conductors. Furthermore, the capacitance associated with each section (disk) was obtained based on the energy method, considering a linear voltage distribution within the sections [13].

Figs. 6 and 7 present comparative analyses of the inductance and resistance values of the first disk based on varying conditions, including air and ferromagnetic cores, with and without accounting for skin and proximity effects in the conductors. The analysis reveals a substantial rise in the resistance due to core losses, outweighing the impact of skin and proximity effects in the conductors. Notably, the inductance values remain significantly higher for the ferromagnetic core, even in the high-frequency domain. This observation, characterized by a high skin depth attributable to the equivalent conductivity of the core material, suggests a notable presence of magnetic flux within the core at high frequencies. While the core's significant impact might suggest that skin and proximity losses in conductors can be reasonably ignored, this conclusion is not strictly correct, as evidenced by the subsequent analysis.

The impedance characteristics of the winding are depicted in Fig. 8 across three scenarios: 1) an air core with skin and proximity effects obtained from FEM analysis, 2) an equivalent iron core with skin and

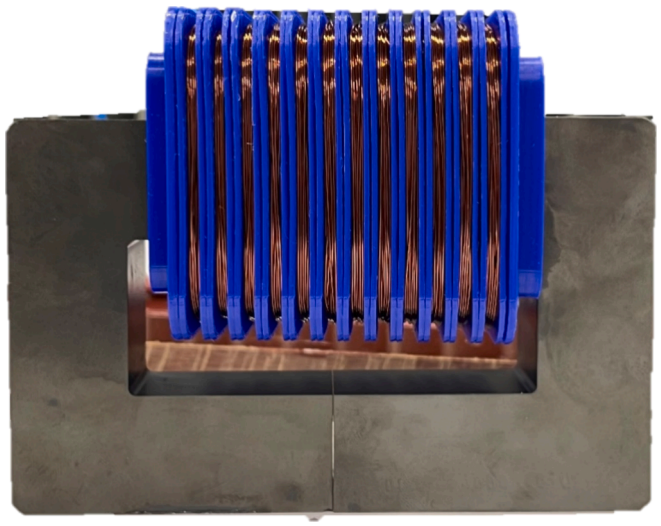

**Fig. 10.** The inductor used for the measurement verification.

proximity effects obtained from FEM analysis, and 3) an equivalent iron core without skin and proximity effects obtained from analytical formulas. Despite significant differences in inductance values between the two core cases, as shown in Fig. 6, a remarkable convergence in characteristics is observed at high frequencies when skin and proximity effects are considered. This convergence suggests that the presence of the core does not influence the high-frequency behavior of transformers.

This phenomenon is related to the phase shifts that occur between different winding sections when the voltage/current wavelength becomes comparable to the winding length. At lower frequencies, the voltages across all winding sections are essentially in phase, resulting in their magnetomotive forces (MMFs) adding up coherently. This produces a significant net MMF that induces substantial magnetic flux linking the core, leading to significant eddy current losses. However, as the frequency increases, propagation delays cause phase shifts between the voltages across different winding sections, akin to the behavior observed in long transmission lines. These phase-shifted voltages produce MMFs in different sections that begin to cancel each other out instead of adding up coherently. Consequently, there is minimal net MMF, leading to very little magnetic flux penetrating the core and drastically reducing the associated eddy current losses in the core material. Thus, the high-frequency response closely mirrors that of an air-core transformer.

To investigate the MMF cancelation, an additional simulation is conducted using COMSOL Multiphysics. The simulation involves the utilization of two disks, as depicted in Fig. 9, to examine the concept. In Fig. 9 (a), both disks are energized with an identical current at a frequency of 1 kHz, resulting in a flux concentration within the core, aligning with expectations. Subsequently, in scenario (b), the currents applied to the disks exhibit a 180-degree phase shift, and as can be seen, most of the flux concentrates between disks, and the iron core influences the flux distribution rather locally. This is similar to the air core scenario shown in Fig. 9 (c). The comparison in Fig. 9 (d) verifies that when there is a phase shift between conductors, the iron core negligibly impacts the inductance and resistance of the segments. It should be noted that the phase shift means the volume confined within the winding is practically shielded from the surrounding magnetic field.

Finally, eddy current losses in conductors completely change the impedance characteristic of the winding. This is again because the behavior of the transformer at high frequencies depends on the differences between the inductive branches rather than their absolute values. While errors in the absolute values of inductances may not be significant, they can be amplified in the difference between them. Hence, it is crucial to consider the eddy current losses in conductors.

## 4. Experimental measurement

To validate the concept of reduced core effects, the impedance of the inductor shown in Fig. 10 is measured in a wide frequency range using ferrite and air cores. The total length of the conductor is around 300 m and the.

measurements are carried out using Omicron Bode 100. Despite ferrite's low conductivity, which can retain the magnetic flux at MHz frequencies, the impedance characteristics for both ferrite and air core configurations exhibit remarkable similarity above 300 kHz, as illustrated in Fig. 11. The similarity of the response between air- and ferrite cores validates the diminished core effects attributed to wavelength effects.

## 5. Conclusion

This paper investigates the high-frequency transformer losses attributed to eddy currents in both conductors and the magnetic core. A comprehensive model of a transformer winding is developed that

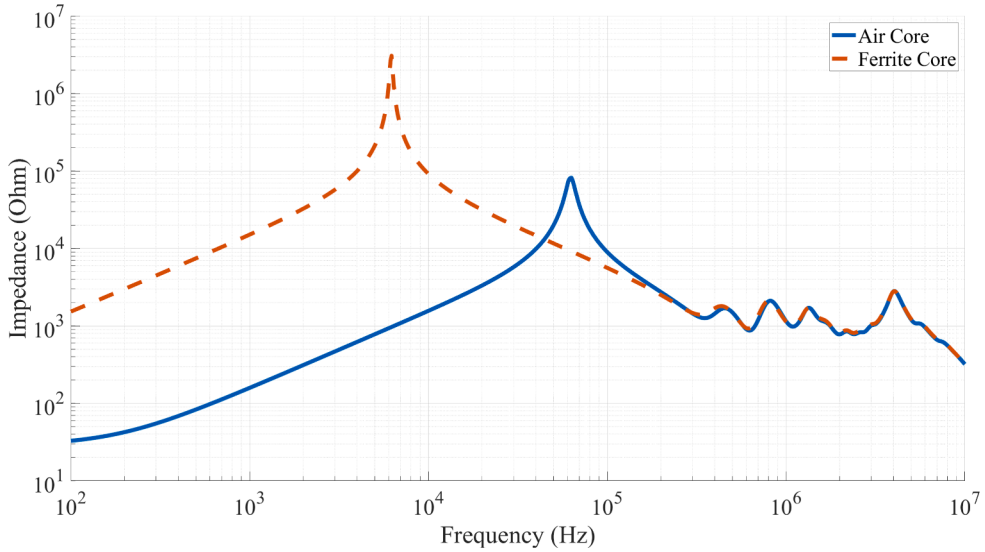


**Fig. 11.** Frequency response of the inductor with air and ferrite cores.

meticulously incorporates skin and proximity effects in the conductors as well as eddy current losses in the core. It is demonstrated through rigorous finite element simulations and empirical measurements that while core losses dominate at lower frequencies, their impact diminishes as the winding length approaches the voltage wavelength at higher frequencies. In such a case, the phase shifts between different winding sections lead to the cancellation of the net magnetomotive force, result in negligible flux in the core. Consequently, the high-frequency impedance characteristics converge remarkably for windings with and without a magnetic core. Furthermore, it is also shown that accurately modeling eddy current losses in the conductors is crucial, as the transient behavior depends on the difference between inductive branches rather than their absolute values. Hence, even small errors in inductance and resistance values can be amplified when their differences are considered. These results can improve transformer design procedures and transient studies involving high frequencies.

## CRediT authorship contribution statement

**Farzad Nasirpour:** Writing – original draft, Visualization, Validation, Software, Methodology, Investigation, Formal analysis, Conceptualization. **Mohamad Ghaffarian Niasar:** Writing – review & editing, Validation, Supervision, Methodology, Investigation, Formal analysis, Conceptualization. **Marjan Popov:** Writing – review & editing, Validation, Supervision, Methodology, Investigation, Formal analysis, Conceptualization.

## Declaration of competing interest

The authors declare that they have no known competing financial interests or personal relationships that could have appeared to influence the work reported in this paper.

## Data availability

No data was used for the research described in the article.

## Acknowledgements

This research work has been financially supported by the Dutch Scientific Council NWO-TTW in collaboration with TSO TenneT, DSO Alliander/Qirion, Royal Smit Transformers, and TSO National Grid, UK, under the project “Protection of Future Power System Components (PRoteuS)”, No. 18699.

## Appendix A

The required functions in (3) are defined as:

$$F_1(\beta_n b) = s\mu_0 \left\{ \frac{f(\beta_n b) - \left(\frac{\mu_0}{\mu_z}\right) f(\Gamma_n b)}{g(\beta_n b) + \left(\frac{\mu_0}{\mu_z}\right) f(\Gamma_n b)} \right\} \tag{11}$$

$$P_1(x,y) = \frac{1}{\beta_n^2 [p_1(x) - p_1(y)]} \tag{12}$$

$$Q_1(x,y) = \frac{2}{\beta_n^2} \left[ \cos\left(\frac{x-y}{2}\right) - \cos\left(\frac{x+y}{2}\right) \right] \tag{13}$$

$$\Gamma_n = \sqrt{\left\{ \frac{\mu_z}{\mu_r} \beta_n^2 + \frac{s\mu_z}{\rho} \right\}} \tag{14}$$

$$f(\gamma) = \gamma \frac{I_0(\gamma)}{I_1(\gamma)} \tag{15}$$

$$g(\gamma) = \gamma \frac{K_0(\gamma)}{K_1(\gamma)} \tag{16}$$

$$p_1(\alpha) = \frac{\pi\alpha}{2} \left[ K_1(\alpha) L_0(\alpha) + L_1(\alpha) K_0(\alpha) \right] \tag{17}$$

where $L_k(\alpha)$ is the modified Struve function.

## References

[1] Gustavsen B, Rahimpour E. High-frequency transformer and reactor models for network studies, part a: white-box models. Conseil Int. des Grands Réseaux Électriques (CIGRE) TB 900 2023:1–203.
[2] Mitchell SD, Oliveira GH. Analysing a power transformer’s internal response to system transients using a hybrid modelling methodology. Int. J. Electr. Power Energy Syst. 2015;69:67–75.
[3] Bjerkan E, Høidalen H. High frequency FEM-based power transformer modeling: Investigation of internal stresses due to network-initiated overvoltages. Electr. Pow. Syst. Res. 2007;77(11):1483–9.
[4] Podoltsev AD, Abeywickrama KNB, Serdyuk YV, Gubanski SM. Multiscale computations of parameters of power transformer windings at high frequencies. Part II: Large-scale level. IEEE Trans. Magn. 2007;43(12):4076–82.
[5] Mitchell SD, Welsh JS. The influence of complex permeability on the broadband frequency response of a power transformer. IEEE Trans. Power Delivery 2009;25 (2):803–13.
[6] Abeywickrama KNB, Daszczynski T, Serdyuk YV, Gubanski SM. Determination of complex permeability of silicon steel for use in high-frequency modeling of power transformers. IEEE Trans. Magn. 2008;44(4):438–44.
[7] Rahimpour E, Christian J, Feser K, Mohseni H. Transfer function method to diagnose axial displacement and radial deformation of transformer windings. IEEE Trans. Power Delivery 2003;18(2):493–505.
[8] Kane MM, Kulkarni S. MTL-based analysis to distinguish high-frequency behavior of interleaved windings in power transformers. IEEE Trans. Power Delivery 2013; 28(4):2291–9.
[9] D. Wilcox, W. Hurley, and M. Conlon, Calculation of self and mutual impedances between sections of transformer windings, *IEE Proceedings C (Generation, Transmission and Distribution)*, 1989, 136 (5) IET, pp. 308-314.

[10] Kiwitt J, Huber A, Reiß K. Modellierung geblechter Eisenkerne durch homogene anisotrope Kerne für dynamische Magnetfeldberechnungen. Electrical engineering (Berlin) 1999;81(6):369–74.
[11] Baravati PR, Moazzami M, Hosseini SMH, Mirzaei HR, Fani B. Achieving the exact equivalent circuit of a large-scale transformer winding using an improved detailed model for partial discharge study. Int. J. Electr. Power Energy Syst. 2022;134:107451.
[12] Jurisic B, Uglesic I, Xemard A, Paladian F. High frequency transformer model derived from limited information about the transformer geometry. Int. J. Electr. Power Energy Syst. 2018;94:300–10.
[13] M. G. Niasar and W. Zhao, Impulse voltage distribution on disk winding: calculation of disk series capacitance using analytical method, *2020 IEEE International Conference on High Voltage Engineering and Application (ICHVE)*, 2020: IEEE, pp. 1-4.